DOI: 10.1002/ ((please add manuscript number))

Article type: Full Paper

Incorporation of Silicon Carbide and Diamond-Like Carbon as Adhesion Promoters Improves *In Vitro* and *In Vivo* Stability of Thin-Film Glassy Carbon ECoG Arrays

Maria Vomero, Elisa Castagnola, Juan S. Ordonez, Stefano Carli, Elena Zucchini, Emma Maggiolini, Calogero Gueli, Noah Goshi, Francesca Ciarpella, Claudia Cea, Luciano Fadiga, Davide Ricci, Sam Kassegne, Thomas Stieglitz*

M. Vomero,

(phone: +49-761-20354041; e-mail: maria.vomero@imtek.de)

Institute of Microsystem Technology (IMTEK), Laboratory for Biomedical Microtechnology, Georges-Koehler-Allee 102 D-79110 Freiburg, Germany

Cluster of Excellence BrainLinks-BrainTools, Georges-Koehler-Allee 80, 79110 Freiburg, Germany

She was with MEMS Research Lab., Department of Mechanical Engineering, College of Engineering, San Diego State University and Center for Sensorimotor Neural Engineering (CSNE) when this project was initiated.

Dr. E. Castagnola,

MEMS Research Lab., Department of Mechanical Engineering, College of Engineering, San Diego State University, 5500 Campanile Drive, San Diego, CA 92182-1323, USA

Center for Sensorimotor Neural Engineering (CSNE), Box 37, 1414 NE 42nd St., Suite 204, Seattle, WA 98105-6271, USA

She was with Center for Translational Neurophysiology of Speech and Communication, Istituto Italiano di Tecnologia when this project was initiated.

Dr. J.S. Ordonez,

Institute of Microsystem Technology (IMTEK), Laboratory for Biomedical Microtechnology, Georges-Koehler-Allee 102 D-79110 Freiburg, Germany

Dr. S. Carli, E. Zucchini, Dr. E. Maggiolini,

Center for Translational Neurophysiology of Speech and Communication, Istituto Italiano di Tecnologia, Via Fossato di Mortara 17/19, 44121, Ferrara, Italy

C. Gueli,

Institute of Microsystem Technology (IMTEK), Laboratory for Biomedical Microtechnology, Georges-Koehler-Allee 102 D-79110 Freiburg, Germany

N. Goshi,

MEMS Research Lab., Department of Mechanical Engineering, College of Engineering, San Diego State University, 5500 Campanile Drive, San Diego, CA 92182-1323, USA

Center for Sensorimotor Neural Engineering (CSNE), Box 37, 1414 NE 42nd St., Suite 204, Seattle, WA 98105-6271, USA

F. Ciarpella,

Center for Translational Neurophysiology of Speech and Communication, Istituto Italiano di Tecnologia, Via Fossato di Mortara 17/19, 44121, Ferrara, Italy

C. Cea,

MEMS Research Lab., Department of Mechanical Engineering, College of Engineering, San Diego State University, 5500 Campanile Drive, San Diego, CA 92182-1323, USA

Center for Sensorimotor Neural Engineering (CSNE), Box 37, 1414 NE 42nd St., Suite 204, Seattle, WA 98105-6271, USA

Prof. L. Fadiga,

Center for Translational Neurophysiology of Speech and Communication, Istituto Italiano di Tecnologia, Via Fossato di Mortara 17/19, 44121, Ferrara, Italy

Section of Human Physiology, University of Ferrara, Via Fossato di Mortara 17/19, 44121, Ferrara, Italy

Dr. D. Ricci,

Center for Translational Neurophysiology of Speech and Communication, Istituto Italiano di Tecnologia, Via Fossato di Mortara 17/19, 44121, Ferrara, Italy

Prof. S. Kassegne,

MEMS Research Lab., Department of Mechanical Engineering, College of Engineering, San Diego State University, 5500 Campanile Drive, San Diego, CA 92182-1323, USA

Center for Sensorimotor Neural Engineering (CSNE), Box 37, 1414 NE 42nd St., Suite 204, Seattle, WA 98105-6271, USA

Prof. T. Stieglitz,

Institute of Microsystem Technology (IMTEK), Laboratory for Biomedical Microtechnology, Georges-Koehler-Allee 102 D-79110 Freiburg, Germany

Cluster of Excellence BrainLinks-BrainTools, Georges-Koehler-Allee 80, 79110 Freiburg, Germany

Keywords: thin-film ECoG arrays, glassy carbon, adhesion promoters, chronic stability, interfaces.

Thin-film neural devices are an appealing alternative to traditional implants, although their chronic stability remains matter of investigation. In this study, a chronically stable class of thin-film devices for electrocorticography is manufactured incorporating silicon carbide and diamond-like carbon as adhesion promoters between glassy carbon (GC) electrodes and polyimide and between GC and platinum traces. The devices are aged in three solutions - phosphate-buffered saline (PBS), 30 mM and 150 mM H_2O_2/PBS - and stressed using cyclic voltammetry (2500 cycles) and 20 million biphasic pulses. Impedance spectroscopy (EIS) and image analysis are performed to detect eventual changes of the electrodes morphology. Results demonstrate that the devices are able to undergo chemically-induced oxidative stress and electrical stimulation without failing but actually improving their electrical performance until a steady-state is reached. Additionally, cell viability tests are carried out to verify the non-cytotoxicity of the materials, before chronically implanting them into rat models. The behavior of the GC electrodes in-vivo is monitored through EIS and sensorimotor evoked potential recordings which confirm that, with GC being activated, impedance lowers and quality of recorded signal improves. Histological analysis of the brain tissue is performed and shows no sign of severe immune reaction to the implant.

1. Introduction

Devices interfacing the nervous system in most cases target long-term (> 1 year) implantations into the hosting body, as their eventual replacement requires surgical intervention,

increases the risk of infections and can lead to the damage of the delicate neural structures. Therefore, any structural change of an implanted device, which is often accompanied by the deterioration of device functionality and the need of replacing it, is to be avoided. [1-4]

In multi-layered, thin-film technology, the stability of the interfaces - especially in a humid environment - strongly depends on the ability of adjacent materials to either chemically interact or mechanically interlock.[5] Multiple aspects of the physics and chemistry of the individual materials are involved in their interaction mechanisms, and define the need for inter-layer adhesion promoter agents.[6, 7] When manufactured with inert and biostable materials, in fact, thin-film devices tend to delaminate over time. Glassy carbon (GC), for instance, is a highly inert material with great potential in the field of neural prostheses, due to its excellent electrochemical properties and resistance to corrosion. However, GC electrodes integrated into thin-film substrates, due to their inertness, do not interconnect strongly with the surrounding materials but could delaminate in the long term (see **Figure S1** in the supporting information section).

Plasma treatments are commonly used in microfabrication techniques for promoting inter-material interactions. Such treatments, in fact, can help to remove contaminants, roughen the treated surface and therefore to promote mechanical and chemical interconnections between adjacent layers. Depending on the chemistry of the plasma, these treatments can create active monolayers by either opening bonds and forming radicals on the substrate material or by electrostatically charging the surface. However, plasma-derived high energy states only last for short time as surfaces tend to relax back to their original state. [8-11] Indeed, electrostatic forces are among the strongest physical attractive forces and are successful for applications in low-humidity environments. In the field of implantable medical systems - where polymer-based carriers are

implanted into the humid body environments - plasma treatments have instead only short term success. Despite different permeation properties, all polymers can be considered transparent to water diffusion during their lifetime into the host body because humidity tends to disrupt electrostatics through charge dissipation leading to the weakening of inter-material bonds strength. [12] Adhesion tests in humid environments have revealed the difference between stability of dry electrostatically active surfaces and the stability of the same material compounds in presence of humidity. [13]

On the other hand, material-deposition processes, like plasma enhanced chemical vapor deposition (PECVD) - and the relatively high energy introduced through plasma deposition and high-voltage particle acceleration - achieve bond formation also between chemically and physically dissimilar layers. In addition, functionally graded multi-layer systems can remain stable in the long-term and in humid environments, which certainly makes them a favorable choice for chronic neural implants. [14] If the materials cohesive energy, their binding state as well as their binding mechanism are dissimilar the chances that they return to a more favorable energetic state over the course of time are high. A system that varies with time is in general undesirable for implantable devices, as it would lack the initial bonded state of the materials and promote delamination and failure of the entire implant in the long term.

Methods to improve the adhesive behavior between materials with different properties - specifically Biphenyltetracarboxylic dianhydride-p-phenylene diamine (BPDA-PPD) polyimide and platinum layers - have been extensively investigated by the authors. Through the use of plasma-deposited silicon carbide and diamond-like carbon, it has been reported that a chemically binding transition between polyimide and platinum-silicide through a silicon carbide interlayer can be

established even upon wet conditions.[15, 16] Plasma enhanced chemical vapor deposition (PECVD) can be achieved through surface reactions by properly choosing the process parameters, therefore it is possible to deposit materials in their most favorable chemical bonding state. In fact, PECVD deposited SiC was investigated and reported in literature also as insulating and mechanically stabilizing coating for platinum and iridium electrodes for cortical recordings[17] other than as biomaterial for chronic neural interfaces[18, 19] due to its robustness and resistance to corrosion, which makes it a great encapsulation layer for implantable devices. Additionally, the concept of graded interfaces for improving the adhesion of polyimide to a polymer of different binding chemistry (silicone rubber) was demonstrated by Ordonez [20].

In the presented work, we investigate whether the integration of silicon carbide and diamond-like carbon as adhesion promoters into flexible thin-film glassy carbon electrocorticography (ECoG) devices can create graded interfaces between glassy carbon electrodes and the surrounding materials and thus result in stable and non-delaminating implantable neural prostheses. Our goal is to establish a stable interface - between glassy carbon electrodes and the subsequent metallic layers, as well as with the polymeric substrate (polyimide) - able to undergo chronic chemical and electrochemical stress without failing. This study covers different in vitro examinations and chronic in vivo experiments to investigate this question.

2. Results and Discussion

2.1. Fabrication

In this work, the interfaces glassy carbon (GC) - metal tracks and GC - polyimide (PI) are studied and optimized for long-term applications of GC-based thin-film neural devices. In fact, the

devices manufactured for this study have GC as electrode material and platinum (Pt) tracks as conductive paths from the electrodes to the rest of the system (connector and electrical system). Metals commonly used in the field of neural prostheses, such as gold and platinum, do not form carbide compounds and are unable to chemically bond with other materials. Therefore, in order to obtain a stable multi-layer device, an adapted MEMS-based interlayer is introduced at the GC-Pt interface. **Figure 1** shows the MEMS process used to manufacture the devices.

Such process is similar to the one described in previous publications by the same authors [21, 22] but differs in the use of silicon carbide (SiC) and diamond-like carbon (DLC) as adhesion promoters in replacement for chromium (Cr). Besides forming a much more stable interface and preventing long-term delamination, SiC and DLC also represent a non-cytotoxic alternative to widely used Cr. A biocompatible metal commonly used as adhesion promoter in thin-film technology for medical devices is titanium (Ti) which, due to its great affinity for carbides and alloys, can be considered as an optional adhesive interface. Nevertheless, an interfacial DLC layer between PI and Ti is believed to be required to avoid the embrittlement of the polymer observed in other studies. [15] In an attempt to achieve the DLC – Ti variation, delamination occurred during an early fabrication stage and manufacturing of comparison devices was not successful. In addition, bi-metal compounds are undesired in the body as they create galvanic cells when reached by water or humidity and can eventually lead to deterioration of the interface through corrosion.

The fabrication process starts with a carbon layer in its sp^2 hybrid chemical state (GC electrodes) followed by DLC - with its mixed sp^2-sp^3 configuration, to which the ability of DLC to irreversibly bond to PI is attributed. [15] For such reason - and with the intent of creating and adhesive transition between GC and PI - the electrodes are coated with DLC before a first layer of PI is spun

over them and patterned, followed by SiC, deposited through plasma enhanced chemical vapor deposition (PECVD). This sequence of materials allows sp^2-sp^2 chemical bonds formation between GC and DLC and, on the other hand, sp^3-sp^3 bonds between DLC and SiC. Pt is then deposited onto SiC and, finally, the graded adhesion sequence is repeated (Si-DLC-SiC) to allow chemical interaction and interlock between metal tracks and the insulative PI layer. A representative of the obtained devices is shown in **Figure 2**.

2.2. Aging and Stimulation

The devices are aged in phosphate buffered saline (PBS), 30 mM H_2O_2 (C1) and 150 mM H_2O_2 (C2), for one week at 39°C and in absence of light, to mimic acute post-surgery inflammatory reaction. When activated, in fact, the immune cells in the brain tissue create a very aggressive chemical environment, rich in digestive enzymes and reactive oxygen species (ROS). [23-25] Hence, hydrogen peroxide is used to test the ability of the thin-film C-based devices to undergo physiological (30 mM, C1) and harsher-than-physiological (150 mM, C2) concentrations. A batch of devices is immersed and aged in PBS as a control and an additional comparison study is carried on using a batch of devices left unaged (Dry). PBS or saline solution is commonly used to test medical devices at elevated temperatures but lacks the presence of ROS and does not capture the harsh in-vivo environment post-implantation. After one week, the 3 aged batches (PBS, C1 and C2) and the one left unaged (Dry) are subjected to 2500 CV (cyclic voltammetry) cycles - between -0.9V and 1.1V, 100 mV/s - to add additional stress and determine whether the devices remain stable under combined chemical and electrochemical load. To monitor their behavior, electrochemical impedance spectroscopy (EIS) measurements are taken after 2500 CV cycles. **Figure 3** shows CV (Figure 3A) and

EIS (Figure 3B) graphs of the 4 categories (Dry, PBS, C1 and C2) at cycle 2500, compared to the EIS and CV of the unaged and unstimulated Dry GC electrode.

Equivalent circuit modelling is used to analyze the experimental EIS data and provide further insight into the charge transfer properties of the electrodes, correlated with the effect of electrochemical stress on their structure. GC electrodes are typically modelled with a modified Randle's circuit, consisting of solution resistance (R_S), a double layer capacitance (C_{dl}) in parallel with the charge transfer resistance (R_{CT}) and the infinite-length Warburg element (W). [21-22, 26] The best agreement between experimental and fitted data, in this case study, is found by adding an additional charge transfer element to the typical circuit model, which is represented in Figure 4B (inset). The need for the additional charge transfer process can be ascribed to the higher porosity exhibited by the GC surface of these electrodes, to the presence of impurities or to the formation of new electroactive site upon electrochemical and/or chemical treatment. [27] Relevant parameters obtained by the fitting are reported in **Table 1**.

The lowest Warburg admittance ($1/Z_W = Y_W = Y_0(iw)^{1/2}$) is exhibited by the pristine GC electrodes and after 2500 CV cycles increases from 0.8 to 1.8 ($nSs^{1/2}$), meaning that electrochemical treatments could be beneficial to pre-activate the GC surface by removing possible impurities or by creating a more porous structure. It has been reported, in fact, that oxidative electrochemical treatments of GC lead to very porous surfaces. [28] The beneficial electrochemical activation of pristine GC can be also observed by the dramatic reduction of the first charge transfer time constant, from 681 ns for pristine GC to 0.78 ns for the electrochemically treated GC. The same electrochemical pathway adopted on GC electrodes aged in PBS produced a more efficient activation of the surface in terms of both a lower resistance to ion diffusion within pores, as expressed by the

lower Warburg impedance, and capacitance, indicating a more porous structure and a larger electroactive area. It is worth noting that the conditions used for the electrochemical stress are very similar to those reported by Heiduschka et al for the electrochemical pretreatment of a GC surfaces. [29] They describe the formation of oxygen-containing groups on the GC surface during the activation process by oxidation of freshly formed carbon at the edge planes. Others have reported that those oxidized films contain quinone-like groups.[30] Additionally, Garzón and co-workers have explained how H_2O_2 treatments on GC can lead to the formation of carboxyls, lactones and phenols.[31] The formation of the same chemical groups is therefore expected on our electrodes surface after oxidative treatments in H_2O_2 and their presence is confirmed by the cathodic and anodic waves in the range -0.5 - +0.5V of the CV, whereas the process at about -0.9V can be attributed to the reduction of carboxylic groups.[32] Surprisingly, we find that the main effect attributable to C1 treatment (30 mM H_2O_2) on GC is the increase of surface roughness, as proved by the upshift of the Warburg parameter Y_W with respect to dry electrodes (1.83 for dry electrodes Vs 4.13 nS $s^{1/2}$ for C1 aged electrodes). More interestingly, the lowest impedance values are observed for electrochemically patterned electrodes that are previously aged in the concentration C2 (150 mM H_2O_2), that enables the formation of a higher activated electroactive surface, as can be also observed by the extremely high capacitance value and by the lowest Warburg impedance. Thus, EIS analysis defines the increased porosity as the most dominant effect of both electrochemical and chemical treatments on the carbon electrodes. This is also confirmed in cyclic voltammetry by the increased capacitance (that can be evaluated by $C = I/\upsilon$ where I is the average current and υ is the scan rate) for electrochemically treated electrodes: it must be pointed out that the same aforementioned

redox active processes (mainly quinone-like and carboxyls) are present for all cases, as can be seen in the CV traces of Figure 3.

GC electrodes are optically analyzed using SEM (scanning electron microscopy) before and after the 2500 CV cycles, to study the effect of electrochemical stress on their structure and correlate eventual change in impedance to the electrode morphology. **Figure 4** shows the representative SEM pictures of GC electrodes after aging (C1, C2, and PBS) and of the Dry control before and after CV. The overall pictures of each electrode are shown in the insets of each category. Since no obvious difference in the morphology of the electrodes can be detected by merely looking at the SEM pictures, they are processed and analyzed using grayscale imaging analysis. Such technique allows the acquisition of specific patterns in the image data and the quantification of porosity on the electrodes surface. Specifically, the *k-means* thresholding method is used for segmenting the grayscale image in 3 different clusters (k=3). Three thresholds are set and three tones of gray are isolated (i.e., light gray, gray, and dark gray). Pores are represented by the pixels belonging to the cluster with the lowest percentage of dark gray. Porosity ratio for each image is defined as the ratio of dark intensity pixels to total pixels. **Figure 5** shows the effect of aging and stimulation on the porosity of GC electrodes. In particular, it is demonstrated that newly fabricated and unstimulated GC electrodes have the lowest porosity ratio. The porosity value increases by 4% for unstimulated electrodes aged in 30 mM H_2O_2 (C1), and dry stimulated electrodes present a 4% higher porosity ratio compared to dry unstimulated electrodes. Porosity significantly rises when more aggressive solutions are used for the aging of the arrays. In fact, unstimulated electrodes immersed in 150 mM H_2O_2 (C2) and electrodes stimulated after aging in 30 mM H_2O_2 (C1) present, respectively, an 8% and 11% increase in porosity ratio compared to dry unstimulated

electrodes. The highest porosity value is calculated for electrodes which are stimulated after aging in 150 mM H_2O_2 (C2). Image analysis and quantification of the surface porosity of the manufactured electrodes proves that their morphology changes consequently to aging in H_2O_2 solutions and to voltage sweep. Interestingly, results show a perfect match between the increase in porosity observed by SEM analysis and the trend observed for the Warburg impedance (Table 1), representing the resistance to diffusion of electrolyte within the surface pores and to/from the bulk solution.

2.3. Biphasic Pulses Stimulation

To establish whether the GC microelectrodes are suitable for cortical stimulation, we investigate their potential to withstand current stimulation patterns. The ability of GC to resist intense and prolonged current stimulation patterns is verified by repeatedly applying a series of 5 million pulses (500 µA current amplitude, 200 µs cathodic half-phase period, 0.2 mC/cm2 charge density) and measuring whether there is any change in impedance spectra after each series. The cathodic charge density applied is within the range of the charge injection limit - defined as the maximum quantity of charge an electrode can inject before reaching the water electrolysis potential. [22] GC electrodes are able to withstand 20 million biphasic pulses with negligible change in EIS, as shown in **Figure 6**. The impedance spectra of GC electrodes before and after biphasic pulses stimulation shows a small reduction of the impedance modulus after the first 5 million pulses, probably due to the well-known phenomena of GC activation. After that initial drop, impedance is stable throughout the rest of the experiment and up to 20 million pulses. The cross section of one stimulated GC electrode (**Figure 7**A) shows that not only GC and PI are strongly bonded through a

thin layer of DLC, but also the Pt metal track and the PI stick perfectly onto each other and do not form any gap (Figure 7B). The electrode side of the devices is optically analyzed using a scanning electron microscope (SEM) and appears smooth and defectless (Figure 7C). The absence of cracks and gaps between GC electrodes and PI substrate is also shown in Figure 7D. Optical microscopy validates these results showing no delamination or failure of the electrodes. [33]

2.4. Cell Viability

Neural interfaces have intimate contact with the brain tissue, thus such devices should have a good interaction with the biological components, in order to limit the inflammatory reaction and toxicity. *In vitro* study of biocompatibility is an important requirement for the safe use of implantable devices and cell culture systems are a simple but effective method that allows to directly measure the cytotoxicity and to determine the effect of a material on cellular growth. In order to verify the non-cytotoxicity of our devices' components, cell viability assay is performed at different time points (5 and 12 days) on the entire microelectrode arrays by monitoring fibroblasts survival. The assay demonstrates that the materials utilized for manufacturing the GC device support both cell adhesion and the cell growth with no significant differences with the control sample. Indeed, the difference between the percentage of surviving cells on the devices and the coverslips is nearly negligible and in both cases the cells viability is very high during the *in vitro* culture (**Figure 8**A). As shown in Figure 8B, the fibroblasts are able to form a thick layer of living cells, as a result of cell proliferation and welfare, confirming the good biocompatibility of the microelectrode arrays.

2.5. SEPs and Chronic *In Vivo* Impedance

ECoG microelectrode arrays are chronically implanted on the somatosensory cortex of 3 rats. Somatosensory evoked potentials (SEPs) elicited by electrical stimulation and *in vivo* impedance spectra are acquired weekly for 6 weeks, to evaluate reliability and stability of the devices during chronic applications. **Figure 9**A reports the averaged somatosensory evoked potentials of 1 rat (n=12 channels) at implant day and after 2, 4 and 6 weeks. During the entire recording session, the ECoG electrode arrays are able to record SEPs elicited with both over-threshold (Figure 9A) and threshold (**Figure S8**) stimulation, assessing their long-term stability even in humid environments. Figure 9B shows *in vivo* impedance spectra (magnitude, mean and standard deviation) of GC microelectrodes the first day of implant and after 2, 4 and 6 weeks after the implant. We can observe that the impedance of the GC micro-electrodes drops within the first 2 weeks from the implantation and subsequently stabilizes and stays constant for the following 4 weeks. Definitely, the *in vivo* behavior is similar to the *in vitro* one, where after an initial activation of the GC electrodes, their electrical properties reach a stable state.

2.6. Optical Analysis Post-Implant

After the 6 weeks, the microelectrodes are explanted and optically analyzed by SEM and via microscope imaging. **Figure 10** reports an optical picture of a micro-ECoG device (A) and a SEM image of one GC electrode after the chronic implantation in the rat model. The SEM picture is taken before cleaning the device. As shown in Figure 10C, it is still possible to see parts of the GC surface, even after 6 weeks into the in-vivo environment, meaning that the electrodes are not fully encapsulated by proteins and isolated from the surrounding tissue. No signs of failure or delamination are observed.

2.7. Histology

Immunofluorescence analysis is performed on 5 rats (3 experimental and 2 control rats) after 6 week long implants since, as many studies report, [3, 34] in case of glial scar formation it is complete after 6 weeks of implantation and remains constant as long as the implant remains in situ. On the control rats, the craniotomy is performed and the skull is subsequently sealed using the same cement and technique used for the actual experiments. However, on the control animals, no device is implanted. In both control and experimental groups, no evidence of glial scar formation is found. When compared to the healthy hemisphere, the level of GFAP for the experimental groups shows 32.5% of intensity, almost comparable with the 24.1% resulting from the control groups. This suggests a non-negligible role in the inflammatory response of the dental acrylic and screws used during the positioning and encapsulation of the devices on the animal skull per se. Additionally, it is interesting to notice that the extension of glial tissue and activated microglia forming from the brain surface is similar for the 2 groups, and measures 143 ± 39.85 µm for the experimental group and 100.2 ± 33.00 µm for the control one. As shown in **Figure 11**C and Figure 11D, GFAP gray scale intensity values of the background are reached within the 200 µm interval. Finally, no difference in ED-1 activation and no neuronal loss is detected (see Figure 11 A, B) for neither of the 2 groups.

3. Conclusion

The intent of the authors is to investigate a new concept of interface, where the best bonding condition between 2 subsequent layers is obtained by adding interlayers of materials acting

as a transitional stage and allowing a graded adhesion mechanism. In particular, such concept is applied here to a new class of thin-film electrocorticography (ECoG) devices made of glassy carbon (GC) electrodes (300 µm diameter) on a flexible substrate of polyimide (PI) with platinum (Pt) tracks for interconnections. The devices are fabricated with the integration of carbon-based adhesion promoters - such as silicon carbide (SiC) and diamond-like carbon (DLC) - with the aim of forming long-lasting chemical bonds between GC electrodes and PI and between GC and Pt. The electrodes are aged in H_2O_2 (30 and 150 mM, concentrations C1 and C2) at 39 °C for a week, to simulated post-surgery inflammatory reaction and verify the stability of the interfaces. After the aging, they are electrochemically stressed with 2500 cycles of cyclic voltammetry and impedance is measured for proving their functionality after both chemical and electrochemical stress. Results show that the electrical performance of the arrays improves after electrochemical stimulation (2500 cycles) proportionally to the amount of H_2O_2 present in the aging solution, due to the activation of the GC electrodes and the probable formation carboxyls, lactones and phenols. The devices are also stressed with 20 million biphasic pulses (500 µA current amplitude, 200 µs cathodic half-phase period, 0.2 mC/cm2 charge density) and similar results are seen: their impedance, measured after every 5 million pulses, tends to decrease until a steady-state is reached. Realistically the steady-state of the pulsed electrodes corresponds to the activated state of the aged and cycled electrodes. SEM pictures - taken before and after the aging test and after the electrochemical stimulation - are analyzed through grayscale image processing that allows the quantification of pores on the electrodes surface. This analysis is concordant with the results obtained from the aging and simulation experiments and shows that the porosity of the GC electrodes increases proportionally to the activation state of the material. The cytotoxicity of the ECoG devices is then tested in fibroblast

cell cultures and excludes the presence of pathogens. Therefore, the electrode arrays are implanted chronically into rat models and tested weekly through impedance measurements. The reported data confirms that, even *in vivo*, the electrodes undergo an activation phase, after which they become much more stable. The quality of the recorded sensorimotor evoked potentials over time improves as well. After 6 weeks, the electrodes are explanted and optically analyzed and show no sign of delamination. Both electrochemical measurements and image analysis state that, after the chronic implants, our devices remain integer. The rats' brains are also histologically analyzed and show no severe reaction to the implanted devices. In conclusion, this study demonstrates that the use of SiC and DLC as adhesion promoters for GC thin-film micro-ECoG electrodes ensures chronic stability of such devices even when tested in very humid and chemically harsh environments. The devices are indeed able to undergo chemical and electrochemical induced oxidation without delaminating or failing.

4. Experimental Section

Fabrication: The fabrication process begins by spin coating a layer of SU-8 (MicroChem, USA) onto a silicon substrate. Photolithography is used to obtain round polymer sections of 300um in diameter on the substrate. These are subsequently pyrolyzed in a furnace (PEO 601, ATV-Technologie GmbH, Germany) at 1000 °C for 60 min, creating the glassy carbon (GC) active sites. GC electrodes are subsequently coated with 50nm of methane-based PECVD diamond-like carbon (DLC), preceded by an argon cleaning step (SCS PCVD REACTOR). Polyimide (U-Varnish, UBE, Japan) is spin-coated onto the substrate and cured at 450°C to a thickness of 5µm, to produce the base layer of the thin-film devices. A second photolithography step is implemented to define 100µm-diameter

openings on the backside of the electrode. These are etched in a reactive oxygen ion plasma to create a port through the polyimide to the underlying DLC layer. After a wet resist stripping, a third photolithography step (AZ5214 Microchemicals GmbH, Germany) is done to define the tracks for electrical routing. Using the same PECVD reactor, argon plasma is used to clean the surface from resist residues and a 50nm layer of silicon carbide is deposited, followed by 300nm of platinum. A 50nm thick layer - transitioning from silicon through SiC to end with DLC - is PECVD-deposited. Another wet resist stripping is followed by a final oxygen and argon plasma clean to remove residues from the resist in between metal lines, previous to the spin-coating of a second layer of polyimide for insulation. Through a final photolithography step and reactive ion etching, the interconnection sites of the electrodes are exposed. Finally, the devices are released from the silicon wafer through a buffered oxide etching process.

Aging: The manufactured devices are divided into 4 groups (5 devices per group) and 3 of the groups immersed into 3 different solutions: phosphate buffered saline (PBS, 0.01 M, pH = 7.4, Sigma Aldrich, USA), 30 mM H_2O_2/PBS (Hydrogen Peroxide 30%, Fisher Scientific, USA) and 150 mM H_2O_2/PBS. The fourth group is left in a dry and protected container and it is used as control (Dry group, unaged). Each device is put in its own beaker, filled with solution (20 ml) and covered with a lid to prevent evaporation. All the beakers are put in a UV-light protected furnace (VWR Scientific ShelLab Sheldon 1415M 9100710 Microprocessor Control Vacuum Oven) with temperature set at 39°C. After 7 days, the devices are taken out of the solutions and characterized in fresh PBS.

Electrode Characterization: The electrochemical behavior of the aged and unaged microelectrodes is studied in 0.01 M PBS (Sigma Aldrich), by electrochemical impedance spectroscopy (EIS) to determine their electrical properties over a large range of frequencies and quantify the effect of chemically-induced oxidative stress on glassy carbon (GC). Cyclic voltammetry is then performed on the GC electrodes 2500 times, and EIS is repeated at the end of the experiment to determine either the electrodes perform in the same way or not. During the CV tests, the working electrode potential is swept between 1.1 and −0.9 V vs. Ag/AgCl, maintaining a scan rate of 100 mV/s. During the EIS measurements, a sine wave (10 mV RMS amplitude) is superimposed onto the open circuit potential while varying the frequency from 1 to 10E6 Hz. Linear sweep voltammetry (LSV) is used for the determination of the water reduction and oxidation overpotentials for the GC electrodes, by sweeping the working electrode potential between -2 and 2 V vs. Ag/AgCl, maintaining a scan rate of 20mV/s. EIS and CV are carried out using a potentiostat/galvanostat (Solartron Analytical, Ametek Scientific Instruments) connected to a three-electrode electrochemical cell with a platinum counter electrode and a Ag/AgCl reference electrode. The software ZSimpWin V 3.2 (EChem Software) is used for equivalent circuit modeling of EIS data.

SEM Imaging/Porosity Analysis: Morphology of GC electrodes prior and after aging and prior and after chronic implant is studied through scanning electron microscopy Zeiss EVO 40 SEM (Zeiss, Germany) in variable pressure mode, using backscattered detector. The average porosity ratio is calculated using a Matlab code that analyzes SEM images of the electrodes. Each SEM image is filtered to remove outliers and then segmented in different classes, sorted from the highest to the lowest intensity grey level by using the *'k-means'* function. For each image, the ratio of the darkest

pixel clusters (which represent the pores of the electrodes) to the total pixels of the image is calculated. Subsequently, for each group of electrodes (Dry unstimulated, Dry stimulated, C1 stimulated, C1 unstimulated, C2 stimulated, C2 unstimulated), the average and standard deviation of the porosity ratios is then calculated.

Electrochemical Biphasic Pulse Stimulation: In order to test the electrochemical stability of the GC microelectrodes, their ability to resist intense and prolonged current stimulation patterns is tested by repeatedly applying a series of five million pulses with 500 µA current amplitude, 200 µs cathodic half-phase period (0.2 mC/cm2 charge density) and a frequency of 1 kHz in saline solution (0.9% w/w NaCl). EIS measurements are taken before starting the stimulation and after each series. EIS measurements are performed by superimposing a sine wave (10 mV RMS amplitude) onto the open circuit potential, in the frequency range from 1 to 10^5 Hz. EIS are carried out using a potentiostat/galvanostat (Reference 600, Gamry Instruments, USA) connected to a three-electrode electrochemical cell with a Pt counter electrode and a Ag|AgCl|KCl(sat.) reference electrode. The integrity of the electrodes was checked through morphological analysis optical microscopy using a Leica Zoom APO 16.

In Vivo Impedance Measurements: In vivo impedances of chronic implanted microelectrodes are analyzed through electrochemical impedance spectroscopy (EIS) using a two-electrode configuration. Each microelectrode is referenced to a low impedance stainless steel bone screw inserted into the skull. The two-electrode method is suitable for measuring impedance from microelectrodes due to the large difference in impedance relative to the reference and the small

current passing through the circuit. [35] During the EIS measurements, a sine wave (10 mV RMS amplitude) is imposed onto the open circuit potential while varying the frequency from 1 to 10^5 Hz. EIS is carried out using a potentiostat/galvanostat (Reference 600, Gamry Instruments, USA). Impedance spectra measurements are repeated three times for each microelectrode at day 1, 7, 14, 21, 28, 35, 42 after implantation.

Cell Culture and Viability Assay: Fibroblast cells are obtained from culture of adult rat tail specimens and used to determine the biocompatibility of the devices, before implantation into animal model. Briefly, tail biopsies (~ 1 cm in length) are obtained from the latter half of the intact tail after skin sterilization with 70% ethanol. Biopsies are further washed in PBS 1X (Thermo Fisher Scientific, US) and cut into small squares (2 × 2 mm^2 approx.) under sterile conditions. 5 to 10 skin pieces are placed in the centre of a 6-well plate covered by a glass coverslip and cultured in Advanced Dulbecco's Modified Eagle Medium (DMEM) (Thermo Fisher Scientific, US) supplemented with 10% Fetal Bovine Serum (Sigma-Aldrich, Italy), 1% penicillin/streptomycin, 1% HEPES and 2mM L-glutamine (all from Thermo Fisher Scientific, USA) at 37°C in a humidified atmosphere of 5% CO_2 in air. The medium is changed every 3 days. Upon confluence, the coverslips are removed and the cells are detached from the plate using 0.25% Trypsin-EDTA (Thermo Fisher Scientific, US) 5 min at room temperature (RT). After centrifugation (1500 rpm, 5 min, RT) the cells concentration is established by counting them in Burker chamber using 0.4% Trypan blue (Thermo Fisher Scientific, US) as vital dye. Fibroblasts were then plated on glass coverslips (control samples) or over the microelectrode array (devices) after surfaces sterilization for 30 min in 70% ethanol followed by washes with PBS. A total of eight devices is used, 4 for each time point with the respective control samples. The cell viability is

analyzed at 5 and 12 days of culture by triple staining with propidium iodide (PI; Sigma-Aldrich, Italy; 5 µg/ml), fluorescein diacetate (FDA; Sigma-Aldrich, Italy; 15 µg/ml) and Hoechst-33342 (Sigma-Aldrich, Italy; 3.3 µg/ml) 3 min at RT in Ringer-Locke solution. After incubation, samples are washed once in Ringer-Locke solution and immediately imaged. Dead cells were visible in red, viable ones appeared in green while total nuclei were stained in blue. At least 10 different fields of view are acquired for each sample. Images are acquired using an Olympus BX51 fluorescence microscope (Olympus, USA) equipped with X-Cite 120 fluorescence illumination system (EXFO, Canada), with a color CX-9000 digital camera (MicroBrightField, USA) coupled with the NeuroLucida software (MicroBrightField, USA). Images are processed and merged using ImageJ (open source NIH image processing software). The percentages of surviving cells (mean ± standard deviation) are calculated based on the ratio of total (Hoechst-positive) nuclei minus PI-positive nuclei (dead cells) divided by the total nuclei.

Animals: Five adult Wistar rats weighing 400-500 g are used for chronic *in vivo* experiments: 3 implanted with the ECoG electrode arrays (experimental rats) and 2 implanted only with dental acrylic and screws (control rats) used as a reference for the tissue damage evaluation. All the experimental subjects were bred in the breeding facility of the University of Ferrara. The experiments are carried out in accordance with the guidelines established by the European Communities Council (Directive 2010/63/EU of September 22nd, 2010) and the protocol is approved by the Italian Ministry of Health, authorization n° 332/2015-PR.

Animal Surgery and Implantation of the Electrodes: Long Evans rats are anesthetized with a mixture of Zoletil (Virbac, France; 30 mg/kg) and Xylazine (Bayer, Germany; 5 mg/kg) administered intraperitoneally (i.p.). For the duration of the whole procedure, the depth of anesthesia is monitored by testing the absence of hind limb withdrawal reflex and is maintained by additional i.m. doses of anesthetic. The body temperature is maintained at 37–38 °C with a thermostatically controlled heating pad, and lacrigel (Farmigea, Italy) is placed on eyes to avoid dryness. After shaving and swabbing the head with ethanol, the anesthetized animal is placed in a stereotaxic apparatus (David Kopf Instruments, USA) equipped with Ear Bars (Model 957 for small animals). An approximately 2 cm long incision is made along the midline of the cranium. The underlying muscle and connective tissue are retracted to expose the skull. A craniotomy (5 x 6 mm^2) is made in the parietal bone to expose the somatosensory cortex identified according to vascular landmarks and stereotaxic coordinates. [36, 37] Sterile saline solution is applied while drilling to avoid any local heating and to keep clean the bone surface. The devices are placed over the dura mater in the S1 cortex area and, after implant, the surface of the implanted tissue is protected using Kwik-Sil silicone polymer (World Precision Instruments Inc, USA). The device is then cemented to the skull using dental acrylic (Jet Repair Acrylic; Lang Dental Manufacturing, USA) and to hold the implant in place, four stainless steel bone screws are inserted into the skull and a stainless steel ground wire is attached to the nearest screw as a reference. The skin is sutured around the cement, gentamycin cream (Milan s.p.a., Italy) is spread over the wound and finally an antibiotic solution of Baytril 5% is administered (Bayer, Germany, 0.5 ml/10 kg, i.m.). The whole procedure is carried out in the same way for both groups of rats (experimental and control rats), a part from the absence of the device in the control rat group.

Electrical Stimulation and SEPs Recordings: Chronic neural recordings (6 weeks) from the somatosensory cortex are performed on 3 rats in order to characterize the electrical performance of the device during *in vivo* long-term application. Specifically, somatosensory evoked potentials (SEPs) from vibrissae cortex are elicited by trigeminal nerve electrical stimulation and the electrophysiological data is acquired weekly. To elicit neural response, two intramuscular bipolar needle electrodes are manually inserted into the vibrissae pad and 102 positive rectangular pulses of 2.5 or 4 mA magnitude (respectively, threshold and over-threshold stimulation) and 0.2 ms duration are generated and delivered every 4 seconds (0.25 Hz)[38] by a WPI A310 pulse generator through a WPI A360R stimulus isolation unit (World Precision Instruments, USA). Neural signals are acquired using TDT multi-channel recording system 3 (Tucker-Davis Technologies, USA) including ZIF-Clip® headstage with unity (1x) gain, the RZ2 real-time processor and the PZ2-256 battery-powered preamplifier. Data is digitized at a sample rate of 3051.8 samples/s at 24-bit resolution, and transferred from RZ2 to the PC by fast fiber optic connection. Then, the acquired traces are digitally low-pass filtered (Butterworth 2nd order) using MATLAB software (Mathworks, USA) to obtain the local field potential (LFP, <300 Hz) and 102 responses are averaged from 50 ms before and 100 ms after stimuli using EEGLAB MATLAB [39] toolbox and OriginPro (OriginLab, USA).

Histology and Immunofluorescence: At the end of the recording sessions (6 weeks), the animals of both groups (experimental and control) are maintained deeply anesthetized and transcardially perfused with 500 ml of 0.1 M sodium phosphate buffered solution (PBS, pH = 7.4) at

room temperature followed by 500 ml cold fixative solution of 2.0% paraformaldehyde, 1.25% glutaraldehyde and 2.0% sucrose (all from VWR, USA), prepared in 500 ml of 0.1 M PBS solution. Brains are then removed, postfixed overnight at 4°C and placed in a 30% sucrose-buffered solution until they sink. They are then frozen and 50 µm-thick coronal sections are cut using a sliding microtome (SM2000R; Leica Microsystems, Canada). In order to investigate the tissue response to the electrode implant, immunofluorescence staining is performed. Brain sections are stained using antibodies directed against: reactive astrocytes detected by the production of glial fibrillary acidic protein (GFAP); activated microglia/macrophages detected by the membrane-bound CD68-antigen (clone-ED1); neuronal nuclei (NeuN) and total number of cell nuclei (DAPI). The adjacent sections are divided into two series, treated with blocking solution consisting of 4% (v/v) normal goat serum (Sigma Aldrich, USA), 0.5% (v/v) Triton-X-100 (Sigma Aldrich, USA), 2% (w/v) bovine serum albumin (BSA) (Sigma Aldrich, USA) in PBS for 1 h and then incubated in the primary antibodies overnight at room temperature. The first series is stained using mouse-anti-GFAP (1:500, Sigma Aldrich, USA) while the second one using mouse-anti-ED1 (1:300, Millipore, USA) and rabbit-anti-NeuN (1:200, Millipore, USA). After 3 rinses in PBS (10 minutes per rinse) the first series is incubated with the antimouse-Alexa-488cojugated secondary antibody (1:500, Thermo Fisher Scientific, USA) while the second one is incubated with the antirabbit-Alexa-488 and antimouse-Alexa-633conjugated secondary antibodies (1:500, Thermo Fisher Scientific, USA) for 4 h in the dark, at room temperature. All mentioned antibodies are used diluted in the blocking solution. Finally, after washing 3 times in PBS, the two series sections are mounted separately onto microscope slides, counterstained with ProLong® Gold Antifade Mountant containing DAPI (Thermo Fisher Scientific, USA) and covered with a cover glass. The staining is observed using an BX51 microscope with 10x,

20x, 40x objectives (Olympus, Japan) and equipped with a X-Cite® 120 fluorescence microscopy illumination system (EXFO, Canada) and a color video camera CX-9000 (MicroBrightField, USA). The images of the fluorescence of the ED1-positive cells (red), GFAP-positive cells (green), neuron nuclei (green) and cell nuclei (blue) are acquired and analysed using NeuroLucida (MicroBrightField, USA) and ImageJ software (developed at the National Institutes of Health, USA). The density of GFAP immunoreactivities of the brain cortex underneath the craniotomy and the intact hemisphere is measured with ImageJ software on images acquired with the same exposure time and using 20x lens for both experimental and control rats. The quantification box that delimited the region of interest is chosen considering the extension of the reactive glia and the same box in the same slice is used to measure the background values captured distant from the brain surface. The density value of the background is then subtracted from the density of GFAP fluorescence. Finally, the percentage of fluorescence gain of the craniotomy hemisphere in respect to the healthy one is calculated in both groups. NeuroLucida software is used to measure the extension of the reactive astrocytes (data presented as mean ± standard deviation).

Statistical Analysis: The data analysis for cyclic voltammetry (CV) and electrochemical impedance spectroscopy (EIS) experiments is carried out using the software OriginPro 2016 (Origin Lab, USA). The sample size for each experimental group is 5 (n=5) and the data (EIS and CTC values) presented as mean ± SD is calculated using the *descriptive statistics* function of OriginPro. Data is not pre-processed. The statistical analysis of the porosity is performed using the software MATLAB (Mathworks, USA), the sample size for each group of images is 5 (n=5) and data is presented as mean ± SD. Before calculating the porosity and starting the segmentation process, each image is filtered by

removing the outliers with the matlab function *remove outliers.m* (see Supplementary Information for details). Somatosensory evoked potential analysis is performed on 3 rats (n=3). The acquired traces are digitally low-pass filtered (<300 Hz, Butterworth, 2nd order) using the software MATLAB (Mathworks, USA) and 100 responses are averaged from 50 ms before to 100 ms after stimuli using EEGLAB MATLAB toolbox. The electrodes of each device (n=12) are then averaged and plotted using OriginPro (OriginLab, USA) for each recording session (day of the implantion and after 2, 4 and 6 weeks). Immunofluorescence analysis is performed on 3 experimental rats and 2 control rats. The images (n=20 for each different stain) are acquired and analysed using the softwares NeuroLucida (MicroBrightField, USA) and ImageJ (developed at the National Institutes of Health, USA). For performing the analysis of the GFAP intensity, the images are background subtracted. Data is presented as mean ± SD. For the viability assay, a total of eight devices is used, 4 for each time point (5 and 12 days) with the respective control samples. For each sample, at least n=10 different fields of view were acquired and processed to evaluate the percentage of surviving cells, reported as mean ± SD. A two-sample (control and device) unrelated two-tailed t-test is used to assess the non-significant difference (P value > 0.05).

Funding: This work was supported by National Science Foundation [grant number EEC-1028725] under the ERC program and by the Cluster of Excellence BrainLinks-BrainTools [DFG, EXC 1086].

Received: ((will be filled in by the editorial staff))
Revised: ((will be filled in by the editorial staff))
Published online: ((will be filled in by the editorial staff))

References

[1] S. F. Cogan, *Annu. Rev. Biomed. Eng.,* **2008**, *10*, 275.

[2] B. Rubehn, T. Stieglitz, *Biomat.,* **2010**, *31*, 3449.

[3] V. S. Polikov, P. A. Tresco, W. M. Reichert, *J. Neurosc. Meth.,* **2005**, *148*, 1.

[4] X. Liu, D. B. McCreery, R. R. Carter, L. A. Bullara, T. G. Yuen, W. F. Agnes, *IEEE Trans. Rehab. Eng.,* **1999**, *7*, 315.

[5] M. Vomero, E. Castagnola, E. Maggiolini, F. Ciarpella, I. Rembado, N. Goshi, L. Fadiga, S. Kassegne, D. Ricci, *Adv. Sci. and Tech*., **2017**, *102*.

[6] S. R. Dupont, M. Oliver, F. C. Krebs, R. H. Dauskardt, *Solar En. Mat. and Sol. Cells,* **2012**, *97*, 171.

[7] J. D. Yeager, D. J. Phillips, D. M. Rector, D. F. Bahr, *MRS Proc.,* **2008**, *1116*, I09.

[8] B. Zhu, H. Iwata, I. Hirata, Y. Ikada, *J. Adhes. Sci. and Tech.,* **2000**, *14*, 351.

[9] A. B. Meddeb, Z. Ounaies, M. Lanagan, *Chem. Phys. Lett.,* **2016**, *649*, 111.

[10] Y. Nakamura, Y. Suzuki, Y. Watanabe, *Thin Sol. Films,* **1996***, 290*, 367.

[11] S. H. Kim, S. W. Na, N. E. Lee, Y. W. Nam, Y. H. Kim, *Surf. and Coat. Tech.,* **2005***, 200*, 2072.

[12] R. Lacombe, *Adhesion measurement methods: theory and practice*, *CRC Press,* **2005**.

[13] L. P. Buchwalter, R. H. Lacombe, *J. Adhes Sci. and Tech.,* **1988**, *2*, 463.

[14] M. Mehregany, C.A. Zorman, N. Rajan, C. H. Wu, *Proc. of the IEEE,* **1998***, 86*, 1594.

[15] J. S. Ordonez, C. Boehler, M. Schuettler, T. Stieglitz, *MRS Proc.,* **2012**, *1466.*

[16] J. S. Ordonez, C. Boehler, M. Schuettler, T. Stieglitz, *Proc. IEEE Eng. in Med. and Biol. Soc. Conf. (EMBC),* **2012**, 5134.

[17] S. F. Cogan, D. J. Edell, A. A. Guzelian, Y. Ping Liu, R. Edell, *J. Biomed. Mat. Res. Part A*, **2003**, *67*, 865.

[18] G. L. Knaack, D. G. McHail, G. Borda, B. Koo, N. Peixoto, S. F. Cogan, T. C Dumas, J. J. Pancrazio, *Front. in Neurosci.,* **2016**, *10*.

[19] C. Diaz-Botia, L. Luna, R. Neely, M. Chamanzan, C. Carraro, J. Carmena, P. Sabes, R. Maboudian, M. Maharbiz, *J. Neu Eng*. **2017**, *14*, 5.

[20] J. S. Ordonez, C. Boehler, M. Schuettler, T. Stieglitz, *Neur. Eng. (NER) 6th Intern. IEEE/EMBS Conf.,* **2013**.

[21] M. Vomero, P. Van Niekerk, V. Nguyen, N. Gong, M. Hirabayashi, A. Cinopri, K. Logan, A. Moghadasi, P. Varma, S. Kassegne, *J. Micromech. and Microeng.* **2016**, *26*, 2.

[22] M. Vomero, E. Castagnola, F. Ciarpella, E. Maggiolini, N. Goshi, E. Zucchini, S. Carli, L. Fadiga, S. Kassegne, D. Ricci, *Sci. Rep*., **2017**, *7*.

[23] J. A. Badwey, M. L. Karnovsky, *Ann. Rev. Biochem.,* **1980***, 49*, 695.

[24] B. Halliwell, *J. Neurochem.,* **1992**, *59*, 1609.

[25] W. Freinbichler, M. A. Colivicchi, C. Stefanini, L. Bianchi, C. Ballini, B. Misini, P. Weinberger, W. Linert, D. Varešlija, K. F. Tipton, L. Della Conte, *Cell. and Molec. Life Sci.,* **2011**, *68*, 2067.

[26] I. D. Raistrick, J. R. Macdonald, D. R. Franceschetti, J. R. MacDonald, *Impedance Spectroscopy: Emphasizing solid materials and systems*, John Wiley & Sons, New York, **1987**.

[27] X. Cui, D. C. Martin, Sens. and Act. A: Physical, **2003**, *103*, 384.

[28] T. Nagaoka, T. Fukunaga, T. Yoshino, I. Watanabe, T. Nakayama, S. Okazaki, *Anal. Chem.,* **1966**, *60*, 2766.

[29] P. Heiduschka, A. W. Munz, W. Göpel, *Electrochim. Acta,* **1994**, *39,* 2207.

[30] A. L. Beilby, T. A. Sasaki, H. M. Stern, *Anal. Chem.,* **1995**, *67*, 976.

[31] F. J. López-Garzón, M. Domingo-García, M. Pérez-Mendoza, P. M. Alvarez, V. Gómez-Serrano, *Langmuir* **2003**, *19*, 2838.

[32] H. P. Dai, K. K. Shiu, J. *Electroanal. Chem*. **1996**, *419*, 1.

[33] M. Vomero, E. Castagnola, J. S. Ordonez, S. Carli, E. Zucchini, E. Maggiolini, C. Gueli, N. Goshi, L. Fadiga, D. Ricci, S. Kassegne, T. Stieglitz, *Neu. Eng. (NER), 8th Intern. IEEE/EMBS Conf*. **2017**.

[34] D. Prodanov, J. Delbeke, *Front. Neurosci*., **2016**, *10*, 11.

[35] E. Castagnola, E. Maggiolini, L. Ceseracciu, F. Ciarpella, E. Zucchini, S. De Faveri, L. Fadiga, D. Ricci, *Front. Neurosci.* **2016**, *10*, 151.

[36] J. K. Chapin , C. S. Lin, *J. Comp. Neurol.* **1984**, *229,* 199.

[37] G. Paxinos, *The Rat Brain in Stereotaxic Coordinates*, 6th Edn. Amsterdam: Elsevier, **2007**.

[38] G. Agrawal, N. V. Thakor, A. H. All, *J. Clin. Neurosci*. **2009**, *16*, 1052.

[39] A. Delorme, S. Makeig, *J. Neurosci. Methods* **2004**, *134*, 9.

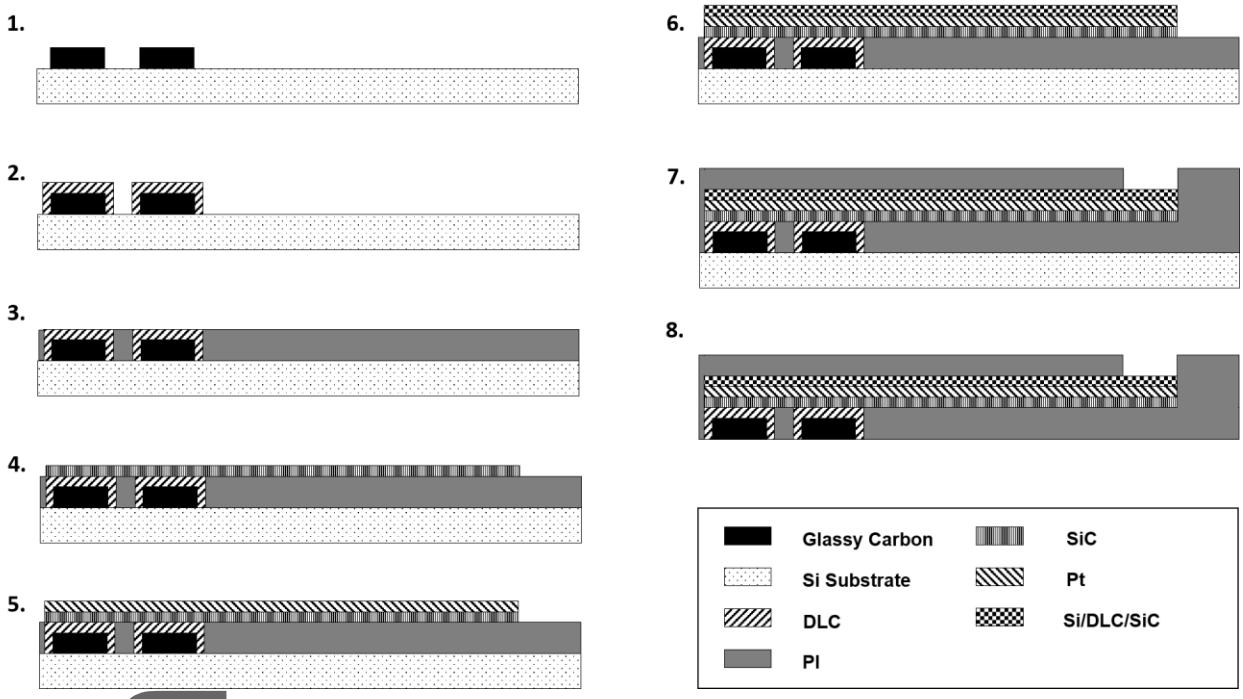

Figure 1. MEMS process for fabricating the multi-layer thin-film glassy carbon (GC) arrays: 1. Fabrication of GC electrodes by pyrolysing 300 µm ⌀ disks of SU-8. 2. PECVD of 50 nm DLC (diamond-like carbon) onto GC electrodes. 3. First layer of polyimide (PI, 5 µm), patterned to open the vias to the GC electrodes. 4. PECVD of 50 nm SiC (silicon carbide) on the tracks of the devices. 5. Sputtered platinum (Pt, 300 nm). 6. PECVD of 50 nm Si/DLC/SiC. 7. Second layer of PI (5 µm), patterned to access the metal bump pads. 8. Buffered Oxide Etch (BOE) for releasing the devices from the substrate.

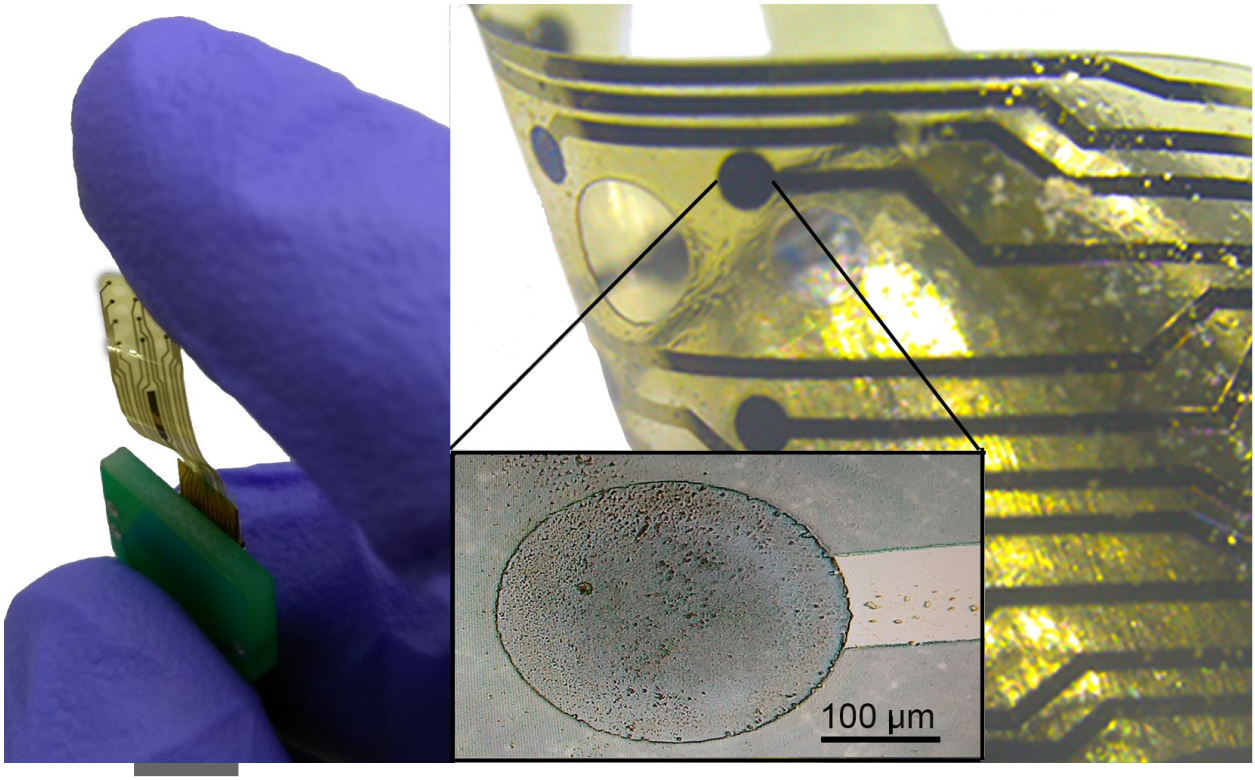

Figure 2. Representative image of a 12-electrode glassy carbon array on polyimide (PI) substrate (left); Detail showing one electrode perfectly embedded into the PI substrate (right).

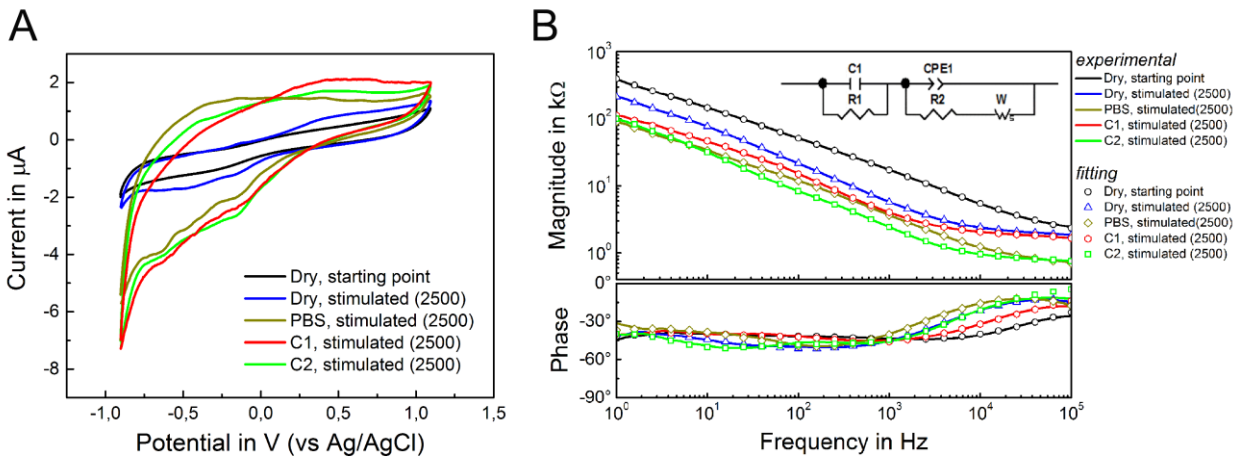

Figure 3. (A) Representative cyclic voltammograms (CVs) of glassy carbon (GC) electrodes belonging to the 4 categories (Dry, PBS, C1 and C2) after 2500 CV cycles, compared to the CV of the untreated and unstimulated Dry GC electrode (starting point). (B) Representative EIS impedance spectra (experimental and fitting) of the same 4 categories compared to the starting point (Dry GC electrodes). The inset reports the equivalent circuit model for GC electrodes.

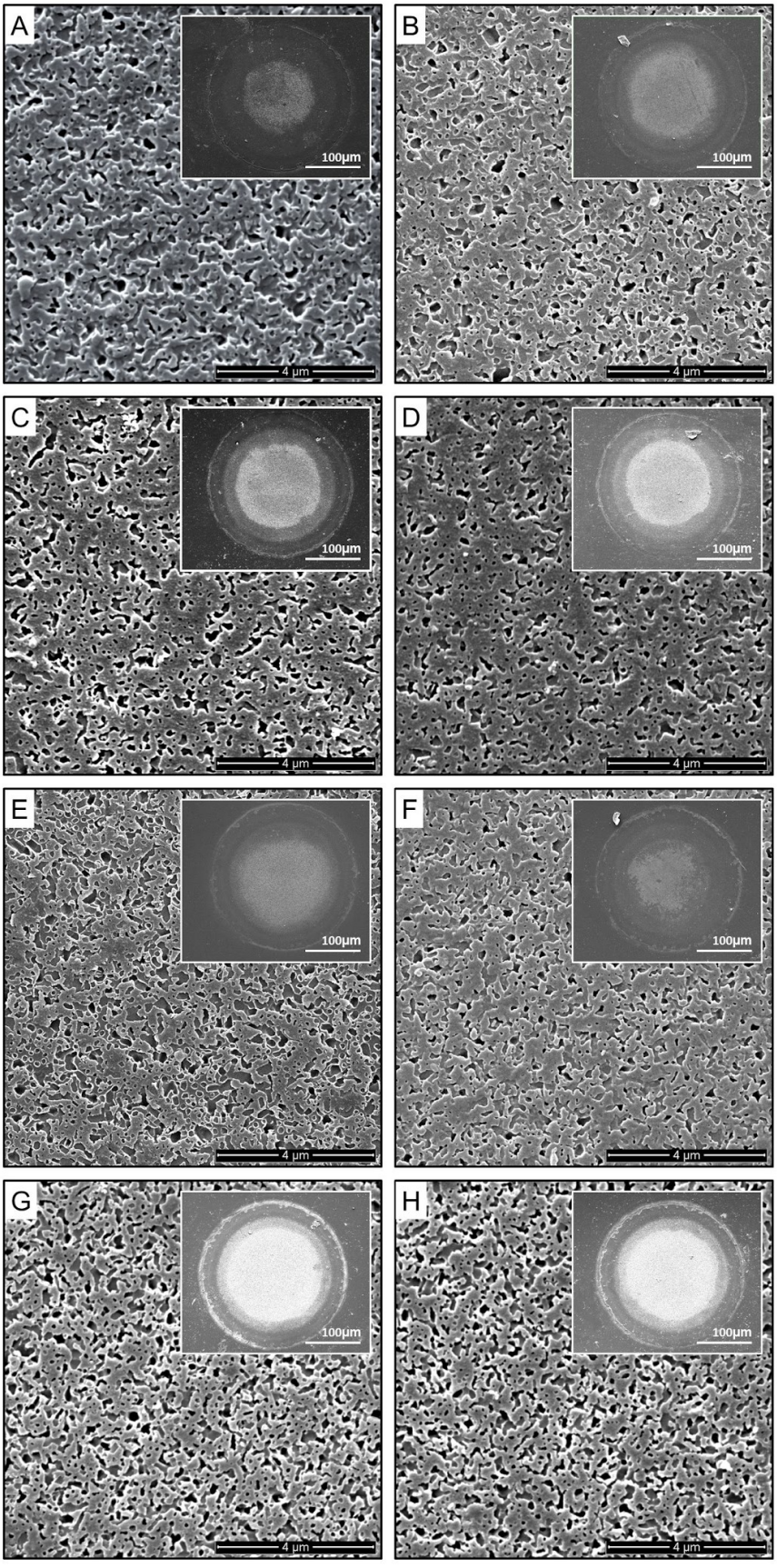

Figure 4. Representative SEM images of glassy carbon electrodes: (A) After fabrication; (B) plus 2500 CV cycles; (C) After 1-week immersion in PBS at 39 ℃; (D) plus 2500 CV cycles; (E) After aging with 30mM H_2O_2; (F) plus 2500 CV cycles; (G). After aging with 150mM H_2O_2; (H) plus 2500 CV cycles.

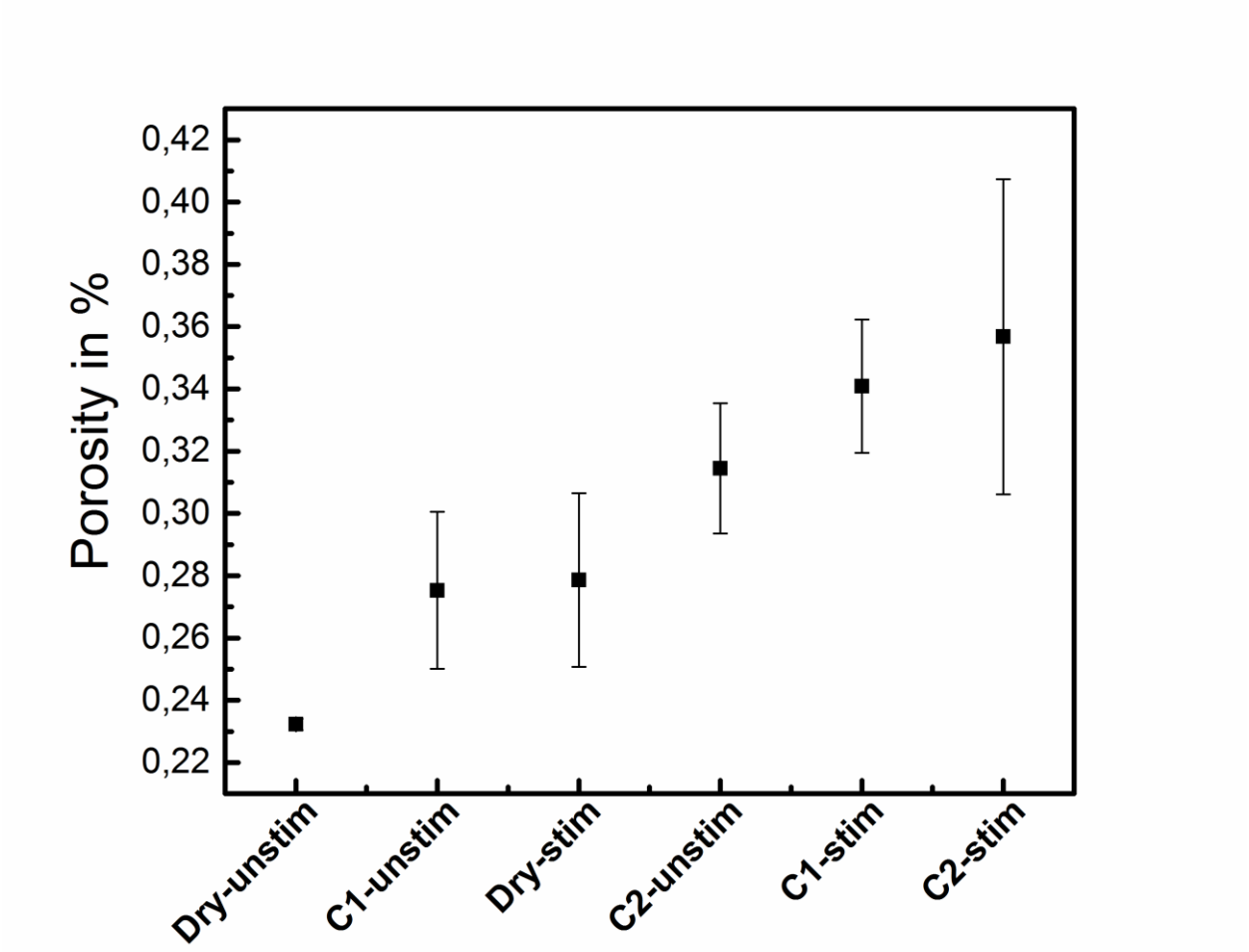

Figure 5. Graph showing the increase of porosity ratio among the groups (n = 5 per group). Dry unstimulated electrodes have the lowest value; unstimulated electrodes immersed in 30 mM H2O2 have an increase of the 4% porosity ratio (C1 unstimulated); dry stimulated electrodes present a 4% higher porosity ratio compared to dry unstimulated electrodes (Dry stimulated); electrodes immersed in 150 mM H_2O_2 have an 8% porosity ratio increase compared to dry unstimulated electrodes (C2 unstimulated); electrodes immersed in 30 mM H_2O_2 solution and stimulated have an 11% increase in porosity ratio compared to dry unstimulated (C1 stimulated); the highest porosity ratio is detected for electrodes which are stimulated and immersed in 150 mM H_2O_2 (C2 stimulated).

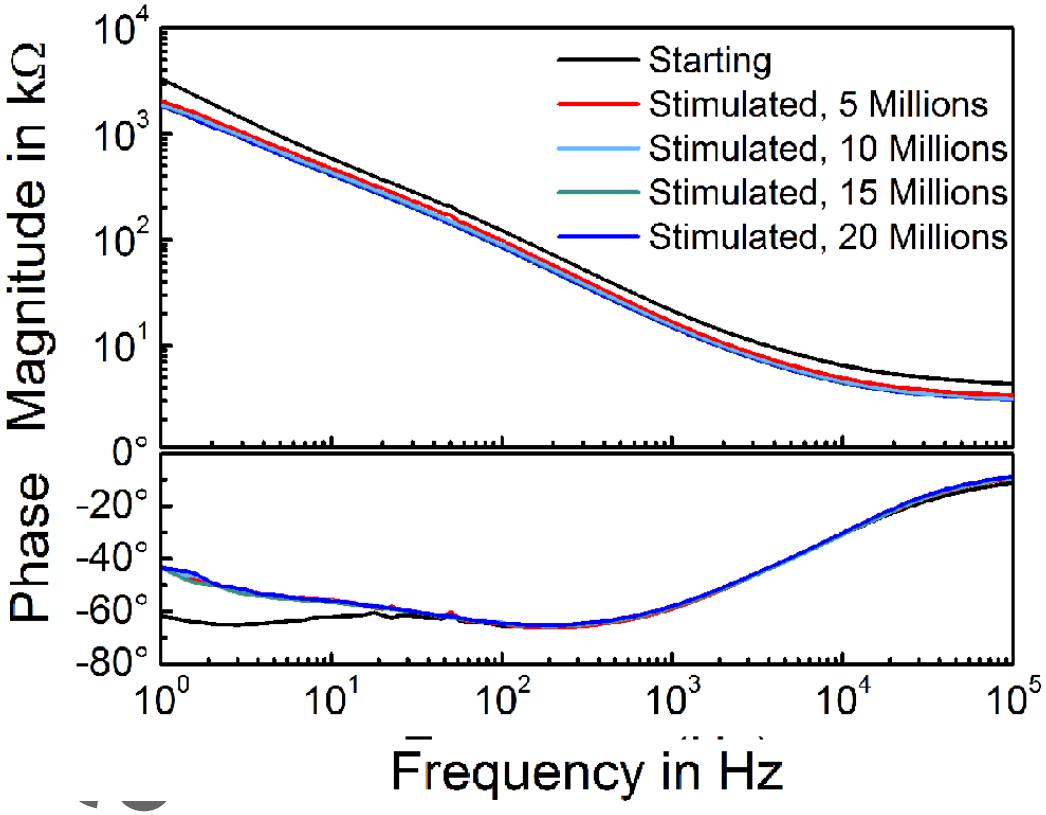

Figure 6. Representative EIS plot of a GC electrode (300 µm dia) stimulated with biphasic pulses (cathodic first, 0.2 mC/cm2) 20 million times.

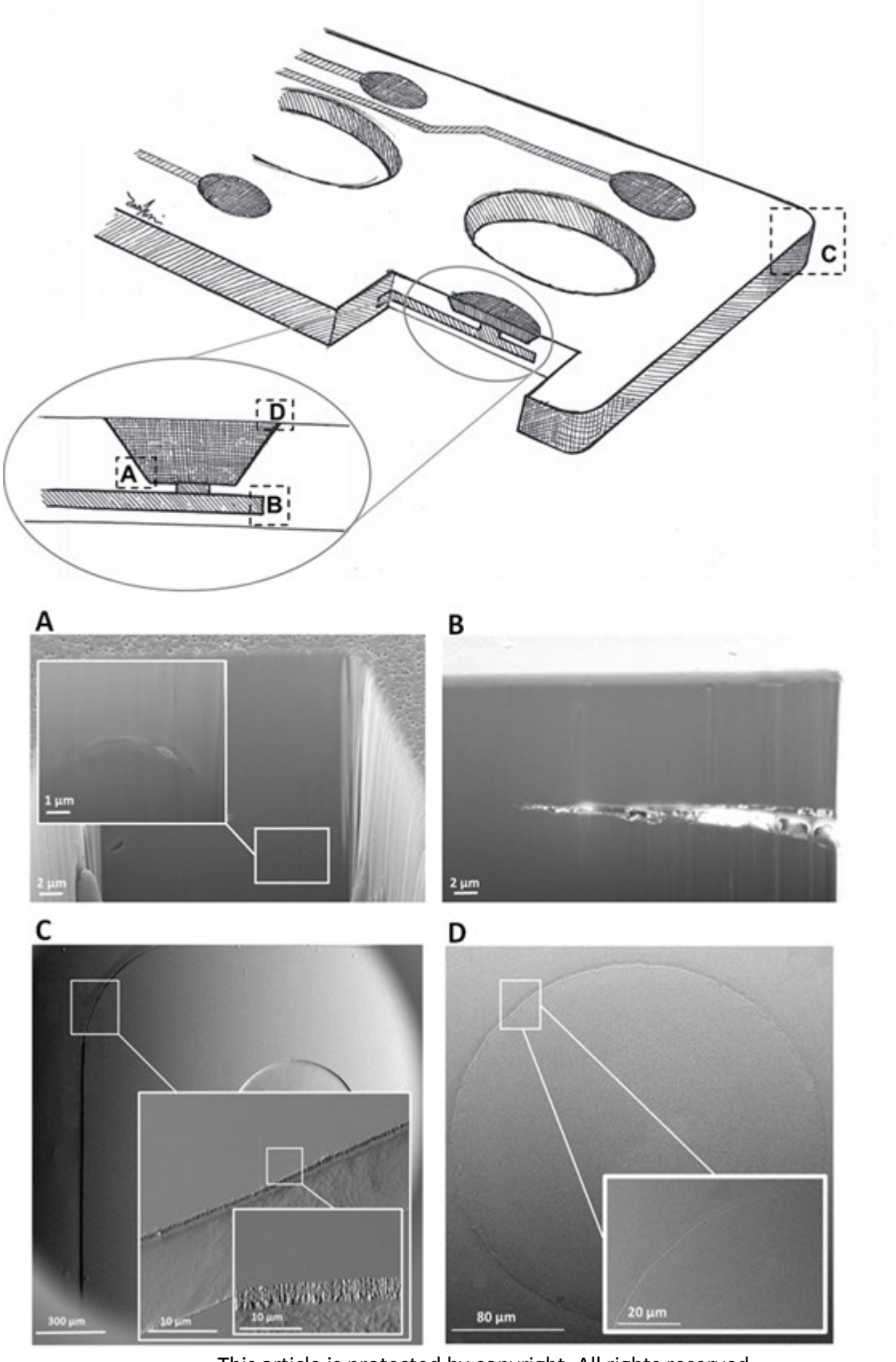

Figure 7. Schematic of a device and some details of a thin-film array after biphasic pulses stimulation: (A) FIB picture of the interface GC/PI; (B) Portion of metal track embedded into PI; (C) SEM picture of PI edge; (D) SEM picture of GC electrode and GC/PI interface (inset).

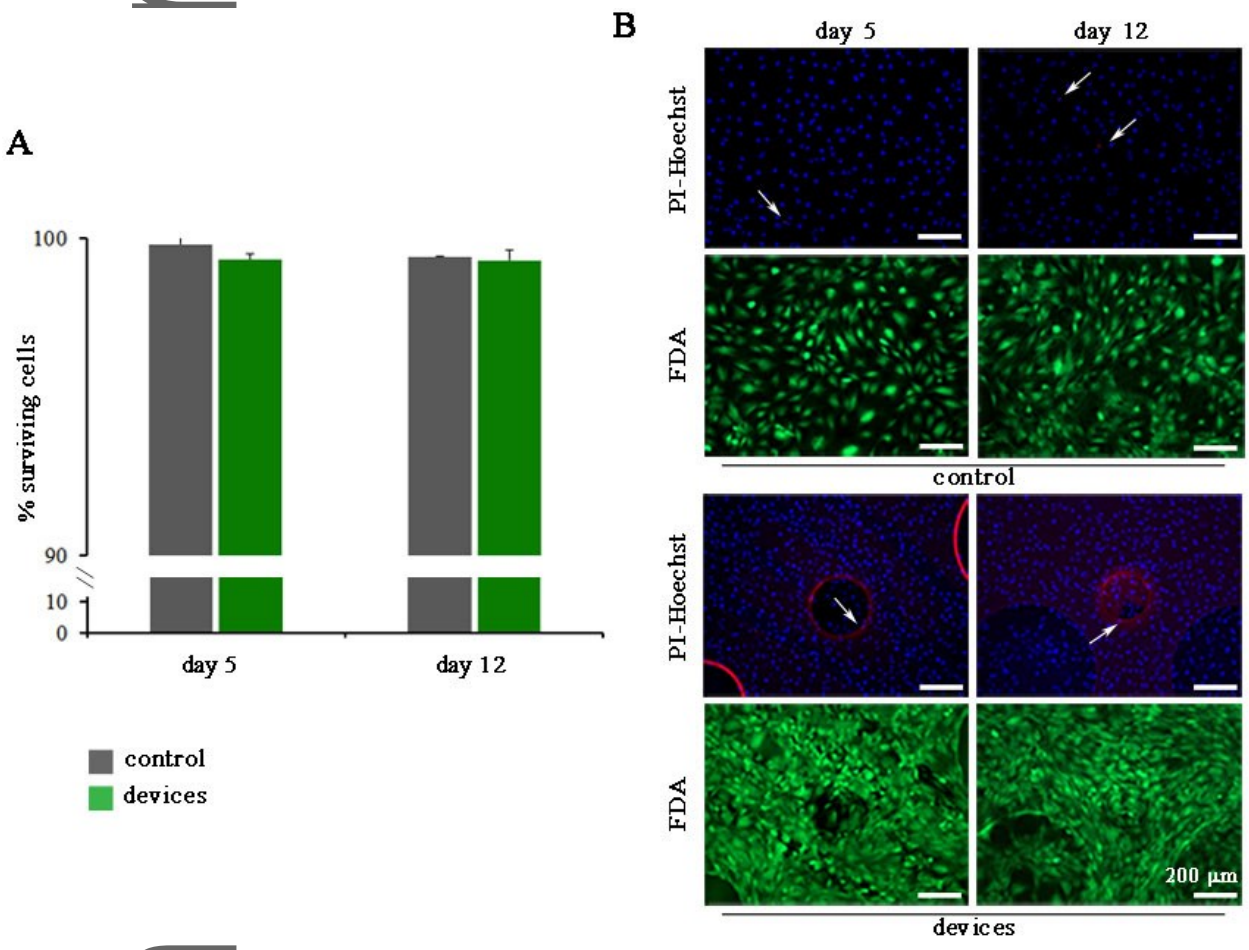

Figure 8. (A) Quantitative analysis of the viability of fibroblasts cells cultured on glass coverslip as control sample (CTR, grey bars) and devices (green bars) at 5 and 12 days in vitro (n = 8). The percentages of surviving cells (means ± SD) were calculated based on the ratio of total (Hoechst-positive) nuclei minus dead cells (PI-positive) nuclei divided by the total nuclei. (B) Representative images of fibroblasts cells grown on glass coverslip (control, upper panel) and devices (lower panel)

at day 5 and day 12 stained with FDA (green-viable cells marker), Hoechst-33342 (blue-total cells nuclei marker) and PI (red-dead cells nuclei marker). White arrows indicate the PI-positive nuclei. Scale bar: 200μm.

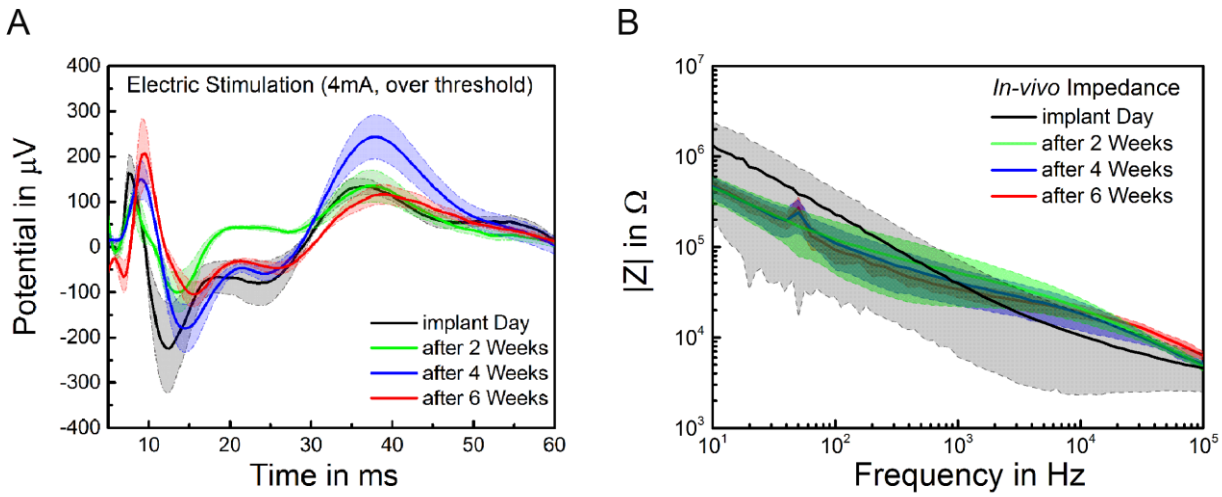

Figure 9. (A) Averaged somatosensory-evoked potentials and standard deviations (n = 12 channels) recorded in response to the electrical stimulation of trigeminal nerves (vibrissa representation) after 100 pulses using 4mA intensity of electrical stimulation. (B) *In vivo* impedance spectra (magnitude, mean and standard deviation) of GC microelectrodes the first day of implant and after 2, 4 and 6 weeks after the implant.

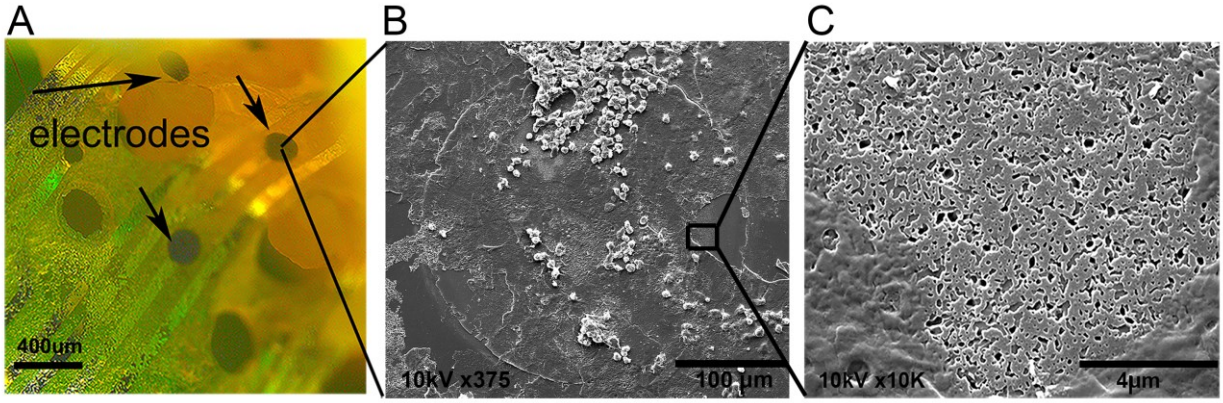

Figure 10. (A) Optical Pictures of micro-ECoG devices after 6 weeks of in-vivo implant. (B, C) SEM images of one GC electrode and its uncovered surface after 6 weeks of in-vivo implant.

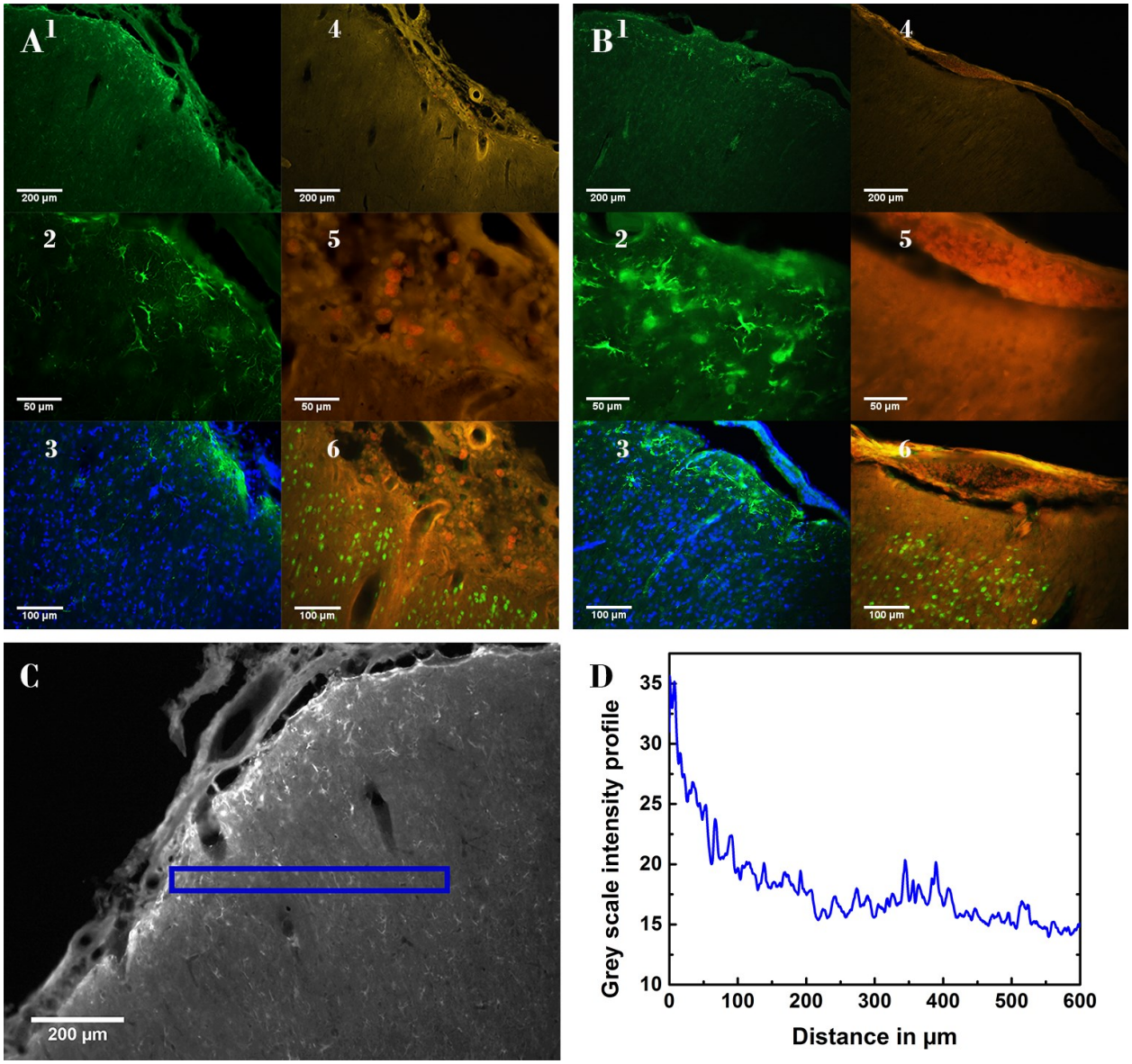

Figure 11. A, B: Fluorescence microscopy images of the implanted cortex area for the experimental rat (A, ECoG electrode array implant) and for the control rat (B, just dental acrylic and screws implant). 1, 2: The images show the GFAP-positive cells (green) at 10x and 40x to underline respectively the morphology of the cortex and of the astrocytes. 3: The images show the cell nuclei (blue) merged on GFAP staining (green) to show the density of DAPI. 4, 5: The images show the ED1-positive cells (red) at 10x and 40x to underline respectively the morphology of the cortex and of the macrophages. 6: The images show the neuronal nuclei (green) merged on ED1 staining (red) to show the density of the neurons under the implanted cortex area. C, D: Fluorescence microscopy image

(C) and the related graph (D) showing an example of the fluorescence (grey scale) decay following the distance from the braìn surface calculated for the blue box area (50x600 µm) shown in panel C.

Table 1. EIS parameters of untreated and unstimulated Dry GC electrode (starting point) and belonging to the 4 categories (Dry, PBS, C1 and C2) after 2500 CV cycles, **obtained by fitting the experimental data to the model shown in Figure 3B (inset)**.

	C	R	τ	Q0	Qn	R	Y0
	[nF]	[kΩ]	[ns]	[10^{-7}S s^n]		[10^5 kΩ]	[nS $s^{1/2}$]
Dry starting	454	21.01	681	2.61	0.61	73	0.82
Dry @2500cv	0.789	0.77	0.78	5.58	0.68	145	1.83
PBS @2500cv	402	1.25	224	21.1	0.58	76	3.26
C1 @ 2500cv	0.802	0.98	0.601	5.82	0.72	56	4.13
C2 @ 2500cv	1929	20.56	1427	6.10	0.75	7	4.50